2024 Tenth Indian Control Conference (ICC)
9 - 11 December, 2024
IISER Bhopal, India

Time Delayed Control for Maneuvering of Magnetic Micro/Nanorobots in Drug Delivering Applications

Neeta Yadav[1], Abhilash Patel[1], Bidyadhar Subudhi[2]

Abstract— **Micro/nanorobots have the potential to revolutionize the medical field by performing tasks such as targeted drug delivery and minimally invasive treatments. For these tasks, path tracking is a critical objective, achievable through closed-loop feedback controllers. However, traditional control methods may be insufficient for accurate tracking, as micro/nanorobots operate in low Reynolds number fluids inside the body, facing various uncertainties and unknown disturbances. To address these challenges, this paper presents a robust adaptive control method for the precise path tracking of microrobots. A time-delayed controller is designed, which utilizes past information to estimate system dynamics uncertainties. The controller parameters, including controller gains and artificial delay values, are obtained using a Lyapunov-Razumikhin-based analysis. This controller design is validated through MATLAB-based simulations and a developed in vitro experimental setup. With the proposed approach, the microrobot is able to track reference trajectories. These results will contribute to advancing robotics applications in the healthcare domain.**

Keywords: Micro/Nanorobots, Targeted drug delivery, Time delayed control, Adaptive control

I. INTRODUCTION

In recent years, the advent of micro/nanorobots has opened up unprecedented possibilities in the medical field. Micro/nanorobots are mobile robots dimensions in the micro/nanometer range and designed for applications where macroscale robots are ineffective or too invasive. These robots have multiple applications in medical fields, such as single-cell manipulation [1], cell transplantation [2], minimally invasive surgery [3], ablation, autopsy, and targeted drug delivery [4]-[5]. Among these, significant attention has been given to targeted drug delivery due to its potential to be an effective treatment for cancer [6]. These micro/nanorobots carry anti-cancer drugs as payload and release on reaching the targeted site. It is essential for targeted drug delivery, these micro/nanorobots should precisely reach the tumor site and robustly deliver the anticancer agents directly to the cancer cells. This is achieved by designing dedicated feedback controllers for maneuvering these robots.

There are diverse actuation methods to navigate the microrobots, such as acoustic waves [7], chemical catalysis [8], light-activated [9], electrical fields [10], and magnetic fields [11]. Magnetic manipulation is a preferred way of actuation for aspects like biocompatibility, deep tissue penetration, precise control, and more degrees of freedom.

This work was supported by IHFC, IIT Delhi

[1] Neeta Yadav and Abhilash Patel are with the Department of Electrical Engineering, IIT Kanpur, Kanpur, India apatel@iitk.ac.in

[2] Bidyadhar Subudhi is with the Department of Electrical Engineering, IIT Goa, Goa, India

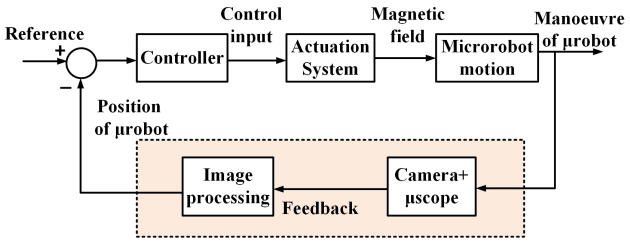


Fig. 1. Block diagram for the maneuvering of magnetic micro/nanorobots.

Typically, the maneuvering of these magnetic microrobots consists of three parts: obtaining position through image processing, magnetic field manipulation, and feedback controller, as shown in Fig. 1. Various *in vivo* imaging techniques [12] help to navigate micro/nanorobots inside the body, and real-time tracking. Magnetic field manipulation is typically done using either a rotating magnetic field or a gradient-based field and to manipulate the field, various control methods have been used to maneuver the microrobots.

Controlling the microrobots through magnetic actuation faces significant challenges due to nonlinearities and uncertainties, including unmodeled dynamics, Brownian motion, and external disturbances like fluid forces, which can compromise control performance. In [13], a proportional controller and in [14], a PID control is employed to control the motion of microrobots. Traditional linear controllers, such as PID, may be insufficient in the presence of highly nonlinear behavior, necessitating the development of advanced nonlinear control strategies. In [15], the A* algorithm based on skeleton extraction was employed to ensure it maintained a safe distance from the vascular wall for safety purposes. Few studies have addressed the adaptive control frameworks, in [16], an augmented error-based model reference adaptive system and in [17], an adaptive backstepping controller for magnetic microrobots and trajectory optimization are discussed. A model-free control method, combining sliding mode control and an extended state observer to handle uncertainties and disturbances is presented in [18]. Despite all the adaptive control methods discussed, there is a gap in the literature regarding estimation of non-linear forces. All the methods discussed above are based on linear parameter estimation that cannot be utilized for nonlinear terms. Also if the conditions are not met results in poor transient behavior. Additionally, these adaptive controllers necessitate intensive computation for online estimation of the parameters.

This paper presents a time-delayed control approach, which estimates the uncertainties using past data measurements and uses it in the control law. Lyapunov Razumikhin-

based analysis was used to design the controller parameters, such as controller gains and artificial time delay value. This method can overcome the above-mentioned problem of intensive computation, and chattering in motion tracking. This controller design is validated in MATLAB simulation and developed experimental setup for *in vitro* manipulation. The results will help towards designing autonomy in microrobots for drug delivery applications.

II. Problem Formulation

A. Modelling

A widely used design of micro/nanorobots for drug delivery applications is a core-shell type spherical shape, made of binding polymers and ferromagnetic materials. In the following, a spherical magnetic microrobot is considered in the scale of $100-200\mu m$. For drug delivery, these micro/nanorobots travel through the blood fluid of arteries and veins, encountering forces such as drag, electrostatic, etc. These forces can be difficult or sometimes impossible to measure. In this work, we consider the motion in $x-y$. For this, dynamical equation of the magnetically actuated micro/nanorobots in the fluid subjected to multiple forces can be given by

$$M\ddot{p} = F_m + F_{drag} + F_\Delta, \tag{1}$$

where $p = [x \quad y]^T$ is the micro/nanorobot position vector, F_{drag} is the drag force exerted on the micro/nanorobot due to the viscous resistance of fluid, which depends on the shape, size, and velocity of the micro/nanorobot. For a sphere of radius r moving with velocity $\dot{p}$, the drag force will be

$$F_{drag} = -6\pi\eta r\dot{p}. \tag{2}$$

The magnetic force F_m is generated by the magnetic field gradients of the electromagnetic coils. This acts as an actuator for the motion of these micro/nanorobots. F_m is given as,

$$F_m = V(m.\nabla)B = V\begin{bmatrix}\frac{\partial B}{\partial x} & \frac{\partial B}{\partial y}\end{bmatrix}^T m, \tag{3}$$

where, m is the total magnetization, B is the magnetic field strength, and V is the volume of the ferromagnetic micro/nanorobot.

To generate the required magnetic field, actuation system can be developed with two pairs of orthogonally placed electromagnetic coils in X and Y axes. The current in the coils is controlled with the DC-DC converter to generate required magnetic field gradient. The dynamics of the actuation system using KVL and Biot Savart's law can be represented as

$$\frac{di}{dt} = \frac{dV_{in}}{L_c} + \frac{iR}{L_c}, \quad \nabla B = \frac{\mu_o N i}{\Delta p} - B_o, \tag{4}$$

where d is the duty ratio and i is the current drawn by the coils. The denominator term Δp is the change in position with respect to centre, $\Delta p = [\Delta x \quad \Delta y]$. The input voltage is V_{in}, the number of turns per coil is N, and L_c, and R are the inductance and resistance of the coil. This electromagnetic coil can maintain a linear relationship between the current and generated magnetic field, as has been shown in the experimental section.

All the uncertainty in these forces, including uncertainties in the viscous drag force due to variations in the shape, size of microrobots, and fluid viscosity, is modeled as a bounded time-dependent external disturbance F_Δ.

To obtain the position and velocity of these microrobots *in vitro*, a microscope is used. The real-time position and velocity are obtained using a camera-integrated microscope, where visual feed is converted into real-time position and velocity using image and signal processing algorithms [19]. For our analysis and design, we assume that computational time for image processing is negligible, compared to the dynamics.

B. Control Objective

A critical goal of drug delivery applications utilizing micro/nanorobots is achieving precise path tracking for efficient drug deliveries. The reference trajectories to be followed by these micro/nanorobots are obtained from diverse motion planning algorithms [20]. The controller will ensure that the micro/nanorobots can track these paths by minimizing the error between the reference and actual trajectories. The reference trajectory $p_r(t)$ that is obtained from path planning, and $p(t)$ is the real-time position of micro/nanorobots. Thus, tracking error $e(t) = p(t) - p_r(t)$ should be zero at large.

The inherent uncertainties and disturbances present within the biological environment can significantly impact the path tracking of micro/nanorobots. To ensure accurate tracking, the control system should be able to estimate these unknown forces and incorporate them into the controller in real-time. In the next section, a time-delayed control approach is discussed, which has the ability to achieve these control goals.

III. Time-Delayed Controller Design

To design time-delayed controller, microrobot motion dynamics can be rewritten as

$$M\ddot{p}(t) + F_\sigma(p,\dot{p}) = F_m(t), \tag{5}$$

where $F_\sigma = -F_{drag} - F_\Delta$ is the sum of all the uncertain and unmodeled forces. If all forces were known, an ideal controller $F_m(t)$ would have been used as given,

$$F_m(t) = Mu(t) + F_\sigma = M(\ddot{p}_r - K_1 e - K_2\dot{e}) + F_\sigma, \tag{6}$$

where, $\ddot{p}_r$ is the reference acceleration, K_1 and K_2 are controllers gain, and error $e = p - p_r$. As F_σ is unknown, this term will be estimated from the previous data [21]. The control input is defined as

$$F_m(t) = Mu(t) + \hat{F}_\sigma, \tag{7}$$

where $u(t)$ is the auxiliary control input, $\hat{F}_\sigma$ is the estimated value of F_σ. This estimation is done from the information of the previous control input and states as follows,

$$\hat{F}_\sigma \cong F_\sigma(p(t-L),\dot{p}(t-L)) = F_m(t-L) - M\ddot{p}(t-L), \tag{8}$$

where L is a constant small time delay. The choice of time delay is crucial for the stability and performance of the

system states. The value of L is mainly taken as multiples of sampling time. In the absence of acceleration measurement, time delayed acceleration vector $\ddot{p}(t-L)$ is obtained through forward difference approximation. The closed loop dynamics is reconstructed from Eqs (5), (7), and (8) as,

$$M\ddot{p} + \bar{F}_\sigma = F_{mL}, \tag{9}$$

where $\bar{F}_\sigma = M\ddot{p}_L - Mu + F_\sigma$ is the time-delayed error (TDE) and F_{mL} is delayed version of F_m. Let $p_r = [x_r \quad y_r]^T$ be the reference trajectory for microrobot and $e(t)$ be tracking error. The auxiliary control input $u(t)$ is chosen as a state feedback controller, given as

$$u(t) = \ddot{p}_r - K_1 e - K_2 \dot{e}. \tag{10}$$

Substituting the delayed version of control input in Eq. (9), the error dynamics can be expressed as

$$\ddot{e} = -K_1 e_L - K_2 \dot{e}_L + \psi, \tag{11}$$

where, $\psi = M^{-1}(\hat{F}_{\sigma L} - \bar{F}_\sigma) + \ddot{p}_{rL} - \ddot{p}_r$ will be the time delayed error and e_L is error of the previous instant. The standard state space representation of the error dynamics would be

$$\dot{e}_1(t) = A_1 e_1(t) + B_1 e_{1L}(t) + B\psi, \tag{12}$$

where, $e_1 = \begin{bmatrix} e \\ \dot{e} \end{bmatrix}$; $A_1 = \begin{bmatrix} 0 & I \\ 0 & 0 \end{bmatrix}$; $B_1 = \begin{bmatrix} 0 & 0 \\ -K_1 & -K_2 \end{bmatrix}$; $B = \begin{bmatrix} 0 & I \end{bmatrix}^T$. The delayed error $e_{1L}(t)$ can be expressed in terms of $e_1(t)$ as $e_{1L}(t) = e_1(t-L) = e_1(t) - \int_{-L}^{0} \dot{e}_1(t+\tau)\, d\tau$. Now, the error dynamics would be,

$$\dot{e}_1(t) = Ae_1(t) - B_1 \int_{-L}^{0} \dot{e}_1(t+\tau)\, d\tau + B\psi, \tag{13}$$

where $A = A_1 + B_1$. While the time-delayed data can help to estimate uncertainty, an inadequate choice of delay can destabilize the closed-loop operation. To ensure stable operation, we will design K_1, K_2 such that delay free system is stable. For these given values of K_1 and K_2, using the Lyapunov-Razamukhin theorem, a bound on possible delay will be obtained, which can be used for TDC.

Theorem 1: [21] From the stability analysis, the system (10) is uniformly ultimately bounded (UUB) for the control input (8), and the maximum delay time $\bar{L}_{max}$ is

$$L < \left(\frac{\lambda_{min}(Q)}{\|E\|} \right) = \bar{L}_{max}, \tag{14}$$

Here, $E = \alpha P B_1 (A_1 P^{-1} A_1^T + B_1 P^{-1} B_1^T + P^{-1}) B_1^T P + 2(r/\alpha)P$, $\alpha > 0$ and $P > 0$. For some $Q > 0$, $A^T P + PA = -Q$ and $\lambda_{min}(Q)$ is the minimum eigen value of Q matrix. The complete proof of the Lyapunov analysis is given in Appendix A. The error bound for the system to be UUB is

$$\bar{r}_o = \gamma + \sqrt{\frac{2\Gamma}{\lambda_{min}\phi} + \gamma^2}, \quad \gamma = \frac{\|B^T P\| \|\psi\|}{\lambda_{min}(\phi)}. \tag{15}$$

As seen from (15), the error bound depends on the time-delayed error (ψ), implying that the tracking accuracy of the controller may deteriorate as the approximation error increases over time. To address this, we used an adaptive law to approximate the time-delayed error.

Assumption: For the stability analysis, TDE is taken as the upper bounded by an unknown scalar θ *i.e* $\|\psi\| \leq \theta$
The modified control law is given as

$$u = u_a + \Delta u, \tag{16}$$

u_a is the same as in (10), and Δu is the additional part that takes care of the TDE. A suitable choice of Δu is based on [22],

$$\triangle u = \begin{cases} -k\hat{\theta}\frac{s}{\|s\|} & \text{if } \|s\| \geq \varepsilon, \\ -k\hat{\theta}\frac{s}{\varepsilon} & \text{if } \|s\| < \varepsilon, \end{cases} \tag{17}$$

where $\varepsilon > 0$, $k > 0$ are scalars quantity, and $s = B^T P e_1$ is directly proportional to tracking error. $\hat{\theta}$ is the switching gain used to tackle the TDE (ψ). The adaptive law to evaluate the $\hat{\theta}$ is as follows

$$\dot{\hat{\theta}} = \begin{cases} \|s\| & \hat{\theta} > \alpha, \\ \alpha & \hat{\theta} \leq \alpha, \end{cases} \tag{18}$$

It is clear from (18) that $\hat{\theta}$ will increase when error increases or error trajectories move away from the surface $s = 0$. Also, the estimation of the switching gain does not depend on any predefined term. By employing the modified control law (16), the error dynamics can be obtained as

$$\ddot{e}(t) = -K_1 e_L - K_2 \dot{e}_L + \psi + \Delta u_L, \tag{19}$$

where Δu_L is the change in auxiliary control input at the previous time instant.

Theorem 2: The system dynamics (9), employing the auxiliary control input given in (16) along with (7), (17) with adaptation law (18) is UUB. A stability analysis for system with adaptive law is given in Appendix B.

IV. Implementation and Validation

A. Simulation results

To validate the theoretical framework, we designed a time-delayed controller for a spherical ferromagnetic microrobot and evaluated the performance through simulation. Here, simulation of the microrobot motion with the proposed control approach has been done on 2-D plane. The list of parameters used for the simulation is given in Table I. The time delay L taken for the simulation is 50 *ms* obtained using (14). The gains of the auxiliary controller are taken $K_1 = 100$ and $K_2 = 15$, other design parameters are $\alpha = 10$, $\varepsilon = 0.01$, and $k = 0.2$.

For simulation purposes, we have considered two sets of references: study 1 is for linear references, $X_r(t) = t$ *mm*, $Y_r(t) = 3 - 1.2t$ *mm*, and study 2 is for a circular reference. To make a circle in $x-y$ plane, references for x and y are $X_r(t) = cos(2\pi t)$, $Y_r(t) = sin(2\pi t)$ *mm*. The circle made

TABLE I
Parameters used for Simulation

Parameter	Value
Microrobot radius (r)	150 μm
Magnetization (m)	1.2×10^6
Initial conditions (x_0, y_0)	1, 2.7 *mm*
ρ_m	7400 kg/m^3
Fluid density (ρ)	1060 kg/m^3
mass (M)	5 $\times10^6$ Kg

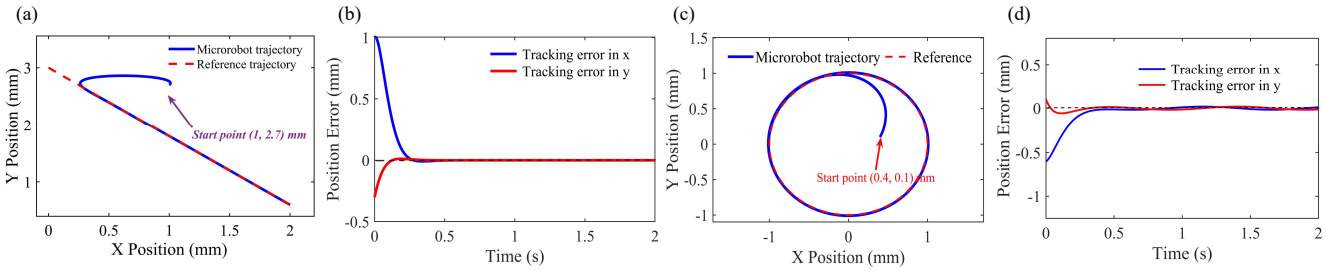


Fig. 2. Simulation results: Blue color line shows the actual trajectory, and dashed red line shows the reference trajectory. (a) $x-y$ trajectory of microrobot for a linear x-y reference (b) Tracking error in x and y for the linear line reference (c) $x-y$ trajectory tracking for circle reference (d) Tracking error in x and y for circle reference

with the chosen reference will be the 1 *mm* radius centered at the origin. With the designed controller, the microrobot was able to track the desired linear reference shown in Fig. 2(a). The error trajectories between the reference and the followed paths of the microrobot are presented in Fig. 2(b). As expected, the error converges to zero as time progresses. The trajectory tracking for the circular path is presented in Fig. 2(c). The tracking error for the circular path is presented in Fig. 2(d).

B. Experimental Setup

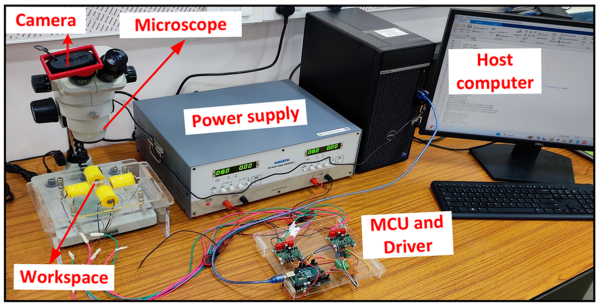


Fig. 3. Experimental setup for the maneuvering of microrobot

To validate the effectiveness of the controller in the presence of real-time forces and disturbances, an experimental setup for the maneuvering of a microrobot has been developed. The complete experimental setup is shown in Fig. 3. The developed magnetic manipulation system is placed on acrylic plates under the microscope. Four orthogonally aligned electromagnetic coils, designed in our lab, are used to maneuver the microrobot on a horizontal plane. Each coil consists of 700 turns of 24 SWG copper wire. The microrobot is kept in a small open petri dish placed in the middle of these four electromagnets. These electromagnets are designed to produce forces along the positive and negative directions of both the x-axis and y-axis with respect to origin. When the microrobot moves along either the x or y direction, only one coil is activated at a time. The coils' current is controlled based on the required magnetic field to drive the microrobot to the desired trajectory. The real-time position of the microrobot feedback is provided with the visual image taken of the workspace with the help of a CCD camera mounted on the microscope. The images are imported into MATLAB, and the image contrast sensitivity method is employed since the microrobot appears darker than background. To accurately detect the center of the microrobot, circular Hough transform [23] has been used. The magnetic actuation setup produces a magnetic field gradient that is effective in a 30×30 mm^2 workspace. The microrobot used throughout the experiment was a 150 μm radius ferromagnetic bead. During experiments, the microrobot is immersed in the fluid inside an open petri dish. To emulate the highly viscous behavior of blood, 100 % glycerol is used.

C. Results and discussion

The sampling time for all the experiments is taken as 50 ms as done in simulation. Time delay (L) is taken as the sampling time as hardware time is less than the sampling time. The camera's frame rate is kept at 20 FPS for real-time position feedback. In line with the simulation, two sets of references are taken for the experiments. For the linear trajectory tracking, the reference in the $x-y$ plane is chosen as a line $(y = mx + C)$. $X_r(t) = 155 + 5t$, $Y_r(t) = 248 + 0.02X_r(t)$ *pixels*. For the circular reference in the xy plane, x and y references are taken as $X_r(t) = 320 + 70 \times cos(2\pi/40t)$, $Y_r(t) = 240 + 70 \times sin(2\pi/40t)$ *pixels*. The center of the circle is kept at $(320, 240)$ *pixels*, which is the center of the 640×480 resolution image. Data acquisition is done every 50 *ms*. The experimental results for the linear $x-y$ trajectory tracking with the adaptive time delay controller is depicted in Fig. 4(a), which is the captured window of the acquired image during the experiment. The tracking error in the x and y directions for linear reference trajectory is shown in Fig. 4(b). The circular trajectory tracking is presented in Fig. 4(c). The error in the x and y directions with respect to the time for the microrobot moving in circular trajectory is shown in Fig. 4(d). The experimental outcomes provide clear evidence of efficacy of the proposed controller. Despite initial deviations and fluid forces, the trajectory consistently aligns with the desired path in less time.

V. Conclusion

This paper presents a robust adaptive control method for path tracking of microrobots operating in complex biological environments. In the proposed adaptive time-delayed control, a state feedback controller and uncertainty of the model is estimated from past measurements. The delay value of this controller is designed using Lyapunov Razumikhin analysis.

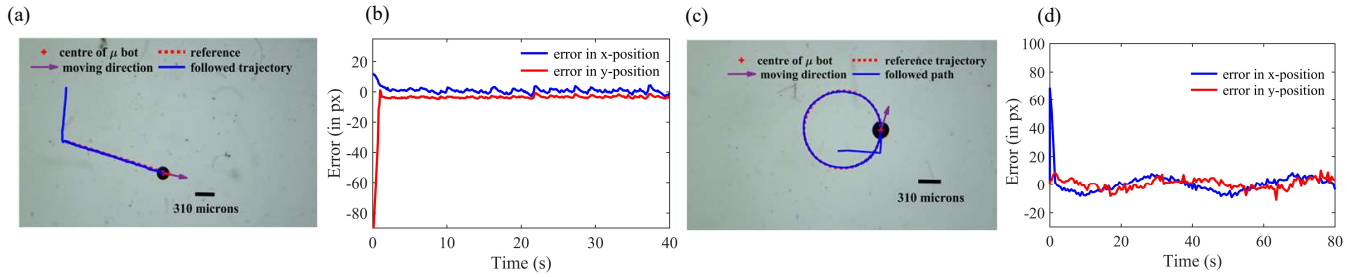


Fig. 4. Experimental results for linear and circular trajectory (in pixels): (a) $x-y$ trajectory tracking for linear reference (b) Tracking error in x and y for linear reference (c) Circular trajectory tracking in $x-y$ (d) Tracking error in x and y for the circular trajectory

The performance of the designed controller is validated through simulations and *in vitro* experiments. The experimental setup was developed in which the current of the electromagnetic coils are manipulated with the controller, and magnetic field gradients generated from these coils control the motion of microrobot. We observed that using TDC the microrobot could track the desired trajectories. This approach paves the way for reliable microrobot control in medical and healthcare applications, offering significant potential for targeted drug delivery and minimally invasive procedures.

APPENDIX A
PROOF OF THEOREM 1

The following proof has been adopted from [22] and modified as per our design requirements.
Define Lyapunov Function $V(e_1)$ as:

$$V(e_1) = \frac{1}{2} e_1^T P e_1. \tag{A.1}$$

The time derivative of (A.1) gives

$$\dot{V}(e_1) = \frac{1}{2}(\dot{e}_1^T P e_1 + e_1^T P \dot{e}_1), \tag{A.2}$$

$$= -\frac{1}{2}(e_1^T Q e_1) - e_1^T P B_1 \int_{-L}^{0} \dot{e}_1(t+\tau)\, d\tau + e_1^T P B \psi \tag{A.3}$$

$s = B^T P e$ By expanding the second term of (A.3) with the help of (11), $\dot{V}$ becomes

$$\dot{V}(e_1) = -\frac{1}{2}(e_1^T Q e_1) - e_1^T P B_1 \left(\int_{-L}^{0} \underbrace{[A_1 e_1(t+\tau)}_{(i)} + \underbrace{B_1 e_1(t-L+\tau)}_{(ii)} + \underbrace{B\psi(t+L)}_{(iii)}] d\tau \right) + s^T \psi. \tag{A.4}$$

By applying the Razumikhin type theorem for the time delay part on (A.4)

$$V(e_1(n)) < rV(e_1(t)) \qquad t - 2L \le n \le t, \quad r > 1$$

and inequality relation of two non-zero vectors

$$z_1^T z_2 \le \alpha z_1^T D^{-1} z_1 + (1/\alpha) z_2^T D z_2.$$

(i) Part of (A.4) will become

$$-2\int_{-L}^{0} e_1^T P B_1 A_1 [e_1(t+\tau)]\, d\tau,$$
$$\le L e_1^T \left[\alpha P B_1 A_1 P^{-1} A_1^T B_1^T P + (r/\alpha) P\right] e_1. \tag{A.5}$$

Similarly, (ii) becomes

$$-2\int_{-L}^{0} e_1^T P B_1 B_1 [e_1(t-L+\tau)]\, d\tau,$$
$$\le L e_1^T \left[\alpha P B_1 B_1 P^{-1} B_1^T B_1^T P + (r/\alpha) P\right] e_1. \tag{A.6}$$

(iii) will be,

$$-2\int_{-L}^{0} e_1^T P B_1 [B\psi(t+\tau)]\, d\tau \le L e_1^T [\alpha P B_1 P^{-1} B_1^T P] e_1 + \int_{-L}^{0} 1/\alpha (B\psi(t+\tau))^T P B \psi(t+\tau)\, d\tau. \tag{A.7}$$

by assuming the system is locally Lipschitz inside the time delay. Let taken the last part as Γ hence, $\|\Gamma\| \le \gamma$.
Now, by substituting (A.6)-(A.7) in (A.4), we have

$$\dot{V}(e_1) = -\frac{1}{2} e_1^T [Q - hE] e_1 + \gamma + \|B^T P\| \|\psi\| \|e_1\|. \tag{A.8}$$

For stability, the condition for time delay is $Q > hE \Longrightarrow \lambda_{min}(Q) > h\|E\|$
Hence, the maximum time delay will be

$$h < \frac{\lambda_{min}(Q)}{\|E\|}. \tag{A.9}$$

Let $\Phi = Q - hE > 0$. The system would be the Ultimate Upper bound by the error bound

$$\bar{r}_o = r_o + \sqrt{\frac{2\gamma}{\lambda_{min}(\Phi)} + r_o^2}, \quad r_o = \frac{\|B^T P\| \|\psi\|}{\lambda_{min}(\phi)}. \tag{A.10}$$

APPENDIX B
PROOF OF THEOREM 2

By taking the Lyapunov function $V_1(e_1)$ for the stability analysis:

$$V_1(e_1) = V(e_1) + \frac{1}{2}(\hat{\theta} - \theta)^2. \tag{B.1}$$

$\dot{V}_1(e_1)$ will be the same as (A.4) with some extra terms as

$$\dot{V}_1(e_1) = \dot{V}(e_1) + s^T \Delta u_L + (\hat{\theta} - \theta)\dot{\hat{\theta}}, \tag{B.2}$$

$$\dot{V}_1(e_1) \leq -\frac{1}{2}e_1^T\Phi e_1 + \gamma + s^T(\Delta u + \psi) + s^T(\Delta u_L - \Delta u) + (\hat{\theta} - \theta)\dot{\hat{\theta}}, \tag{B.3}$$

By taking $\Theta = \Delta u_L - \Delta u$

$$\dot{V}_1(e_1) \leq -\frac{1}{2}e_1^T\Phi e_1 + \gamma + s^T(\Delta u + \psi) + s^T\Theta + (\hat{\theta} - \theta)\dot{\hat{\theta}}. \tag{B.4}$$

1) By taking condition $\hat{\theta} > \alpha$, and $\|s\| \geq \varepsilon$

$$\dot{V}_1(e_1) \leq -\frac{1}{2}e_1^T\Phi e_1 + \gamma + s^T(-k\hat{\theta}\frac{s}{\|s\|} + \psi) + s^T\Theta + (\hat{\theta} - \theta)\|s\|, \tag{B.5}$$

$$\leq -\frac{1}{2}e_1^T\Phi e_1 + \gamma - (k-1)\hat{\theta}\|s\| + \|s\|\|\Theta\|. \tag{B.6}$$

if $\alpha > 0$, then $\dot{V}_1(e_1) < 0$ for the error bound of

$$\bar{r}_1 = \sqrt{\frac{2\gamma\lambda_{min}(\Phi) + (\|\Theta\|\|B^TP\|)^2}{\{\lambda_{min}(\Phi)\}^2}} + \frac{\|\Theta\|\|B^TP\|}{\lambda_{min}(\Phi)}. \tag{B.7}$$

2) Similarly, for $\hat{\theta} \leq \alpha$, and $\|s\| \geq \varepsilon$, error bound will be

$$\bar{r}_2 = \sqrt{\frac{2(\gamma + \alpha^2)\lambda_{min}(\Phi) + ((\theta + \|\Theta\|)\|B^TP\|)^2}{\{\lambda_{min}(\Phi)\}^2}} + \frac{(\theta + \|\Theta\|)\|B^TP\|}{\lambda_{min}(\Phi)}. \tag{B.8}$$

3) For $\|s\| < \varepsilon$, the error is already bounded within the region ε.

REFERENCES

[1] S. Sakar, E. Steager, D. Kim, M. J. Kim, G. Pappas, and V. Kumar, "Single cell manipulation using ferromagnetic composite microtransporters," *Applied Physics Letters*, vol. 96, no. 4, p. 043705, 2010.

[2] S. Jeon, S. Kim, S. Ha, S. Lee, E. Kim, S. Y. Kim, S. H. Park, J. H. Jeon, S. W. Kim, C. Moon, B. J. Nelson, J. young Kim, S. W. Yu, and H. Choi, "Magnetically actuated microrobots as a platform for stem cell transplantation," *Science Robotics*, vol. 4, no. 30, p. eaav4317, 2019.

[3] F. Ullrich, C. Bergeles, J. Pokki, O. Ergeneman, S. Erni, G. Chatzipirpiridis, S. Pané, C. Framme, and B. J. Nelson, "Mobility experiments with microrobots for minimally invasive intraocular surgery," *Investigative Ophthalmology & Visual Science*, vol. 54, no. 4, pp. 2853–2863, 2013.

[4] X. Z. Chen, M. Hoop, N. Shamsudhin, T. Huang, B. Özkale, Q. Li, E. Siringil, F. Mushtaq, L. Di Tizio, B. J. Nelson, and S. Pané, "Hybrid magnetoelectric nanowires for nanorobotic applications: fabrication, magnetoelectric coupling, and magnetically assisted in vitro targeted drug delivery," *Advanced Materials*, vol. 29, no. 8, p. 1605458, 2017.

[5] M. Hoop, F. Mushtaq, C. Hurter, X. Z. Chen, B. J. Nelson, and S. Pané, "A smart multifunctional drug delivery nanoplatform for targeting cancer cells," *Nanoscale*, vol. 8, no. 25, pp. 12 723–12 728, 2016.

[6] F. S. van Dam, W. Boogerd, S. B. Schagen, M. J. Muller, M. E. Droogleever F., E. Wall, and S. Rodenhuis, "Impairment of cognitive function in women receiving adjuvant treatment for high-risk breast cancer: High-dose versus standard-dose Chemotherapy," *JNCI: Journal of the National Cancer Institute*, vol. 90, no. 3, pp. 210–218, 1998.

[7] A. Aghakhani, O. Yasa, P. Wrede, and M. Sitti, "Acoustically powered surface-slipping mobile microrobots," *Proceedings of the National Academy of Sciences*, vol. 117, no. 7, pp. 3469–3477, 2020.

[8] S. Nain and N. Sharma, "Propulsion of an artificial nanoswimmer: a comprehensive review," *Frontiers in Life Science*, vol. 8, no. 1, pp. 2–17, 2015.

[9] W. Yang, X. Wang, Z. Wang, W. Liang, and Z. Ge, "Light-powered microrobots: recent progress and future challenges," *Optics and Lasers in Engineering*, vol. 161, p. 107380, 2023.

[10] S. T. Chang, V. N. Paunov, D. N. Petsev, and O. D. Velev, "Remotely powered self-propelling particles and micropumps based on miniature diodes," *Nature Materials*, vol. 6, no. 3, pp. 235–240, 2007.

[11] G. Go, H. Choi, S. Jeong, C. Lee, B. J. Park, S. Y. Ko, J. O. Park, and S. Park, "Position-based magnetic field control for an electromagnetic actuated microrobot system," *Sensors and Actuators A: Physical*, vol. 205, pp. 215–223, 2014.

[12] X. Liu, Y. Jing, C. Xu, X. Wang, X. Xie, Y. Zhu, L. Dai, H. Wang, L. Wang, and S. Yu, "Medical imaging technology for micro/-nanorobots," *Nanomaterials*, vol. 13, no. 21, 2023.

[13] D. Agarwal, A. D. Thakur, and A. Thakur, "A feedback-based manoeuvre planner for nonprehensile magnetic micromanipulation of large microscopic biological objects," *Robotics and Autonomous Systems*, vol. 148, p. 103941, 2022.

[14] L. Yang, Q. Wang, and L. Zhang, "Model-free trajectory tracking control of two-particle magnetic microrobot," *IEEE Transactions on Nanotechnology*, vol. 17, no. 4, pp. 697–700, 2018.

[15] Z. Huan, W. Ma, J. Wang, and F. Wu, "Path planning and optimization for micro-robot in a vessel-mimic environment," *Frontiers in Neurorobotics*, vol. 16, p. 923348, 2022.

[16] M. B. Khamesee, N. Kato, Y. Nomura, and T. Nakamura, "Performance improvement of a magnetically levitated microrobot using an adaptive control," in *Proceedings International Conference on MEMS, NANO and Smart Systems*. IEEE, 2003, pp. 332–338.

[17] L. Arcese, M. Fruchard, and A. Ferreira, "Adaptive controller and observer for a magnetic microrobot," *IEEE Transactions on Robotics*, vol. 29, no. 4, pp. 1060–1067, 2013.

[18] K. Meng, Y. Jia, H. Yang, F. Niu, Y. Wang, and D. Sun, "Motion planning and robust control for the endovascular navigation of a microrobot," *IEEE Transactions on Industrial Informatics*, vol. 16, no. 7, pp. 4557–4566, 2020.

[19] C. Bergeles, G. Fagogenis, J. J. Abbott, and B. J. Nelson, "Tracking intraocular microdevices based on colorspace evaluation and statistical color/shape information," in *2009 IEEE International Conference on Robotics and Automation (ICRA)*. IEEE, 2009, pp. 3934–3939.

[20] M. Salehizadeh and E. D. Diller, "Path planning and tracking for an underactuated two-microrobot system," *IEEE Robotics and Automation Letters*, vol. 6, no. 2, pp. 2674–2681, 2021.

[21] S. Roy, I. N. Kar, J. Lee, and M. Jin, "Adaptive-robust time-delay control for a class of uncertain Euler–Lagrange systems," *IEEE Transactions on Industrial Electronics*, vol. 64, no. 9, pp. 7109–7119, 2017.

[22] S. Roy and I. N. Kar, "Adaptive-robust control of uncertain Euler-Lagrange systems with past data: A time-delayed approach," in *2016 IEEE International Conference on Robotics and Automation (ICRA)*. IEEE, 2016, pp. 5715–5720.

[23] Z. Yao and W. Yi, "Curvature aided Hough transform for circle detection," *Expert Systems with Applications*, vol. 51, pp. 26–33, 2016.